Asian Journal of Chemistry; Vol. 36, No. 4 (2024), 943-947

ASIAN JOURNAL OF CHEMISTRY

https://doi.org/10.14233/ajchem.2024.31287

Isolation of Verimol G from *Illicium verum* Hook.f. Fruit and its Computational Prediction as Antimalarial Agent

A.N. KRISTANTI[1,2,*], N.S. AMINAH[1,2], T.C. BRAMAYUDHA[1], K.W. MUKHAROMAH[1], A.P. WARDANA[3], B. ILHAM[1] and Y. TAKAYA[4]

[1]Department of Chemistry, Faculty of Science and Technology, Universitas Airlangga, Surabaya, Indonesia
[2]Biotechnology of Tropical Medicinal Plants Research Group, Universitas Airlangga, Surabaya, Indonesia
[3]Department of Chemistry, Faculty of Mathematics and Natural Sciences, Universitas Negeri Surabaya, Surabaya, Indonesia
[4]Faculty of Pharmacy, Meijo University, Nagoya, Japan

*Corresponding author: Fax: +62 31 5936502; Tel: +62 31 5936501; E-mail: alfinda-n-k@fst.unair.ac.id

Received: 25 January 2024; *Accepted*: 8 March 2024; *Published online*: 30 March 2024; AJC-21595

The present research focused on the isolation of the major compound in *Illicium verum* Hook.f. fruit and exploring its potential as an inhibitor of *Plasmodium falciparum* through computational approach, molecular docking and dynamic simulation. Verimol G was successfully extracted from the ethyl acetate extract for the first time from fruit. A successful prediction of the preferred orientation of the ligand to the receptor has been determined by the docking molecular approach. A molecular dynamics simulation was also conducted to study the dynamic behaviour of verimol G in relation to wild-type *P. falciparum* dihydrofolate reductase (PfDHFR). The free binding energy analyses (ΔG_{bind}) of verimol G-PfDHRF was found to be -8.07 kcal mol^{-1}. The decomposition energy results ($\Delta G_{bind}^{residue}$) showed that there were seven key binding residues which stabilized the binding of verimol G. The anticipated data could potentially serve as valuable insights for the advancement and formulation of an antiplasmodial medicine.

Keywords: Antiplasmodial, *Plasmodium falciparum*, Dihydrofolate reductase (DHFR), Molecular docking, Dynamic simulation.

INTRODUCTION

The genus of *Illicium* belongs to the Illiciaceae family. About 40 species of this genus have been found in north-eastern America, Mexico, the west Indies and eastern Asia. Several species of this genus have been used as traditional medicinal plants to treat pain, rheumatism, skin inflammation, *etc.* [1]. They are a rich source of prenylated C6-C3 compounds, neolignans and secoprezizaane-type sesquiterpenes. Such compounds belong to unique structural types and occur exclusively in *Illicium* species and are considered to be characteristic chemical markers [2].

Illicium verum is a medium-sized plant and known as star anise. Star anise is mainly found in east and southeast Asia and southern North America. In east Asia, China is the main production area of star anise, followed by Vietnam, Cambodia, Myanmar, Indonesia and Philippines [3]. The main part of the plant that has high efficacy is the fruit, which is star-shaped in diameter 2.5 cm-4.5 cm. This fruit produces star anise oil which is widely used in the food and pharmaceutical industries because of its antimicrobial, antifungal and antioxidant properties [3,4]. *trans*-Anethole (89.5%), 2-(1-cyclopentenyl)furan (0.9%) and *cis*-anethole (0.7%) were found to be the main components among 22 identified compounds, which accounted for 94.6% of the total oil [4]. Several extracts of *I. verum* Hook. f. fruit have capabilities as an antioxidant, antimicrobial and antiglycemic [5-7].

From literature review, it was found that there are no significant data reports on secondary metabolite chemicals present in the fruit of this plant other than essential oils. On the other hand, no evidence has been found that this genus impacts malaria; however, traditional herbal medicine can become a sustainable source of treatment [8-10]. Thus, traditional medicine has to be taken into consideration while developing antimalarial pharmaceuticals because it provides availability as well as provides effective prevention. Molecular screening through computer aided drug design has become an effective method for identifying the prospective therapeutic candidates to treat different

kinds of diseases. This theoretical approach allows us to get the experimental overview predictability [11,12].

The main purpose of this study was to isolate and elucidate the major secondary metabolite compound structurally from *I. verum* Hook. f. fruit. Moreover, the inhibition activity of an isolated compound as a potential antiplasmodial agent using a computational method was also predicted.

EXPERIMENTAL

The IR spectra was recorded using Bruker ALPHA II – Eco ATR instrument, whereas the UV-VIS spectra was recorded using Shimadzu-1800, Japan. The NMR spectra was recorded with ^{1}H and ^{13}C NMR Bruker 600 MHz at 298 K in DMSO-d_6 solvent. The vacuum liquid chromatographic (VLC) separation and gravity column chromatography (GCC) was performed on silica gel 60 GF_{254} (Merck) and 0.063-0.200 mm, respectively. TLC plates were precoated with 60 GF_{254} (Merck, 0.25 mm) and anisaldehyde as spraying agent was used to detect the spot.

Extraction and isolation: The dried fruit of *I. verum* (1.2 kg) was thoroughly grounded to be a powder and then extracted with ethanol. The extract was evaporated to obtain the concentrated ethanol extract. The ethanolic extract was partitioned with *n*-hexane and ethyl acetate sequentially. After that it was again concentrated by a rotary vacuum evaporator. Next, the ethyl acetate extract was separated by GCC using *n*-hexane: ethyl acetate eluent. The fraction contained pure compound was identified using spectroscopic methods including UV-Vis, IR and NMR.

Docking studies: The obtained compound was designed using the Hyperchem program and then optimized using the Gaussian program. The geometry optimization and calculation were carried out using the DFT method with B3LYP/6-311 ++G** model as the basis-set calculation. Meanwhile, wild-type *Plasmodium falciparum* dihydrofolate reductase-thymidylate synthase (PfDHFR-TS) (PDB ID: 1J3I) was chosen as target protein. Despite the fact that there were four chains, only chain A was utilized in order to avoid the complication. The standard missing residue reconstruction was performed using Modeller 9.21 package. On both ligand and receptor, it was added H-bond atoms and charge by using AMBER FF14SB force field model and AM1-BCC [13,14]. The molecular docking of the isolated compound was performed using the Dock6 package [15]. Some parameters used into the grid-box preparation were grid-spacing (0.3 Å), centre (X: 28.017, Y: 8.509, Z: 57.986) and dimensions (X: 26.738, Y: 23.785, Z: 27.784). To ensure each parameter used, redocking of protein native ligand, WRA, was conducted to evaluate the docking model acceptability based on RMSD value < 2 Å [16].

Molecular dynamic simulations: Molecular dynamic simulations were performed using the Amber22 package [17] for the following complexes (a) free protein (APO), (b) protein co-crystal PfDHFR-TS with WRA inhibitor and (c) verimol G-protein complex after docking. All these complexes were solvated separately by applying them through solvate box TIP3PBOX (size 12 Å). In addition to the model, the protein-ligand, Cl^- and Na^+ ions were added to make the system's total charge neutral by using SIRAH force field [18]. Afterward, the energy system was minimized for 2000 steps before the production stage was carried out for 100 ns. The system was heated and kept at 300 K and 1 atm. The results were analyzed using several variables such as conformation dynamics, binding affinity and key binding residue.

Free energy binding: Using a hybrid-based approach, the binding free energy calculation (ΔG_{bind}) utilized the last 10 ns trajectory from 100 ns. The enthalpy calculation (ΔH) used the Quantum Mechanics/Molecular Mechanics-Generalized Born (QM/MM-GBSA) [19]. Some parameters like generalized born solvation model and QM theory: MNDO method was provided in this research [20]. Meanwhile, the entropy change ($-T\Delta S$) was calculated in the normal mode method (NMODE) [21-24].

$$\Delta G_{bind} = G_{complex} - (G_{receptor} - G_{ligand}) \quad (1)$$

$$\Delta G_{bind} = \Delta H - T\Delta S = \Delta G_{gas} + \Delta G_{sol} - T\Delta S \quad (2)$$

$$\Delta G_{gas} = E_{pl}^{int} \quad (3)$$

$$\Delta G_{sol} = \Delta G_{GB} + \Delta G_{SCF} \quad (4)$$

RESULTS AND DISCUSSION

Spectroscopic techniques were used to elucidate the structure of the isolated compound and the results indicated that the isolated compound was verimol G (Fig. 1), which is agreement with the reported values [25].

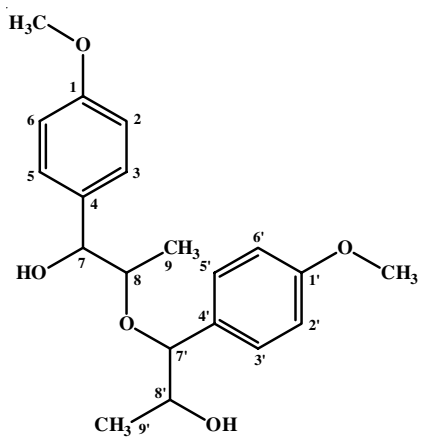

Fig. 1. Molecule structure of Verimol G

Binding and free energy: To investigate the potential compound, the isolated compound was docked (Fig. 2) into the active site of *P. falciparum* dihydrofolate reductase (PfDHFR) [26]. Ligand molecules were superposed and the obtained good criteria RMSD 0.765 Å. The lower interaction energy (Fig. 2d) belonged to the native ligand, WRA (6,6-dimethyl-1-[3-(2,4,5-trichlorophenoxy)propoxy]-1,6-dihydro-1,3,5-triazine-2,4-diamine), indicated a good stability and the binding interaction was more potent than verimol G. The grid scores were calculated from energy of van der Waals (E_{vdW}) and electrostatic (E_{ele}) in gas phase [27]. The E_{vdW} provide a notable contribution to interaction energy against PfDHFR. Afterwards, the free energy binding analysis (ΔG_{bind}) was performed to explore the binding affinity. It used MMPBSA.py tools, which were

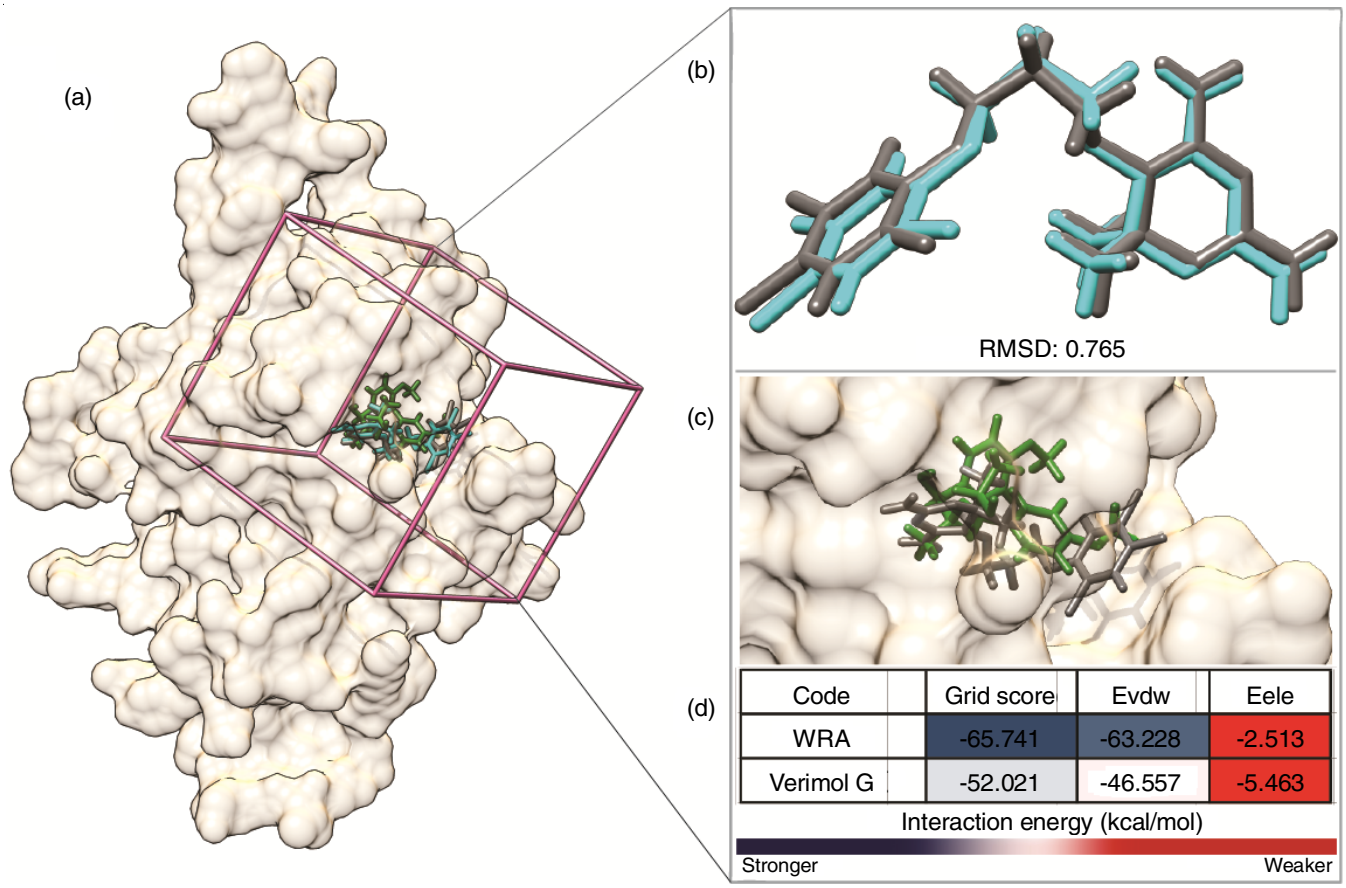

Fig 2. (a) Grid-box coordinate based on native ligand, (b) Redocking analysis based on superposition between co-crystal (cyan) and pose (grey) and (c) ligand pose (d) ligand-receptor docking based on their grid score function (E_{vdw} + E_{ele})

executed from the last 10 ns trajectories. Energy components are listed in Table-1, which shows that WRA has the lowest free binding energy then verimol G. Thus, the binding energy belonging to WRA had more robust binding than Verimol G.

TABLE-1
ENERGY COMPONENTS (kcal mol^{-1}) OF EACH SYSTEM CALCULATED USING QM/MM-GBSA APPROACH

Energy components	WRA	Verimol G
QM/MM (MNDO)		
ΔE_{vdW}	-46.70 ± 0.21	-36.19 ± 0.38
ΔE_{ele}	0.12 ± 0.00	0.22 ± 0.00
ΔG_{gas}	-46.58 ± 0.21	-35.96 ± 0.38
ΔG_{SCF}	-6.10 ± 0.26	0.39 ± 0.26
GBSA		
ΔG_{sol}^{ele}	17.85 ± 0.22	10.61 ± 0.25
$\Delta G_{solv}^{nonpolar}$	-5.26 ± 0.01	-5.15 ± 0.04
ΔG_{sol}	12.58 ± 0.21	5.46 ± 0.22
NMODE		
-TΔS	-23.78 ± 0.80	-22.04 ± 0.96
Hybrid-based binding free energy		
ΔH	-40.10 ± 0.24	-30.11 ± 0.38
ΔG_{bind}	-16.3	-8.07

Dynamics conformation after simulation: Stability and flexibility: This analysis was performed to learn the dynamics behaviour in molecular dynamics simulation [28]. APO PfDHFR was also performed in this study. During simulation as shown in Fig. 3, complex RMSD of all ligands and APO was maintained at 0.35-0.4 nm and 0.2-0.34 nm in the backbone. There was no significant fluctuation shown, which was < 0.4 nm. Each system quickly increased during first 3 ns (2 ns in backbone protein) and then fluctuated by nearly 0.4 ns until 100 ns. Specifically, the last 20 ns trajectory showed good stability. Further analysis was done to learn the effect of ligand on the atom dynamics using root mean square fluctuation

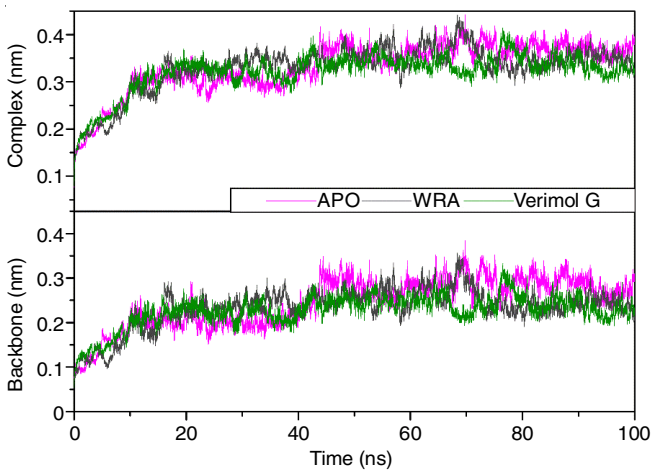

Fig. 3. The-root-mean-square-deviation (RMSD) of Backbone (left) and complex (right) for each system during 100 ns MD simulation

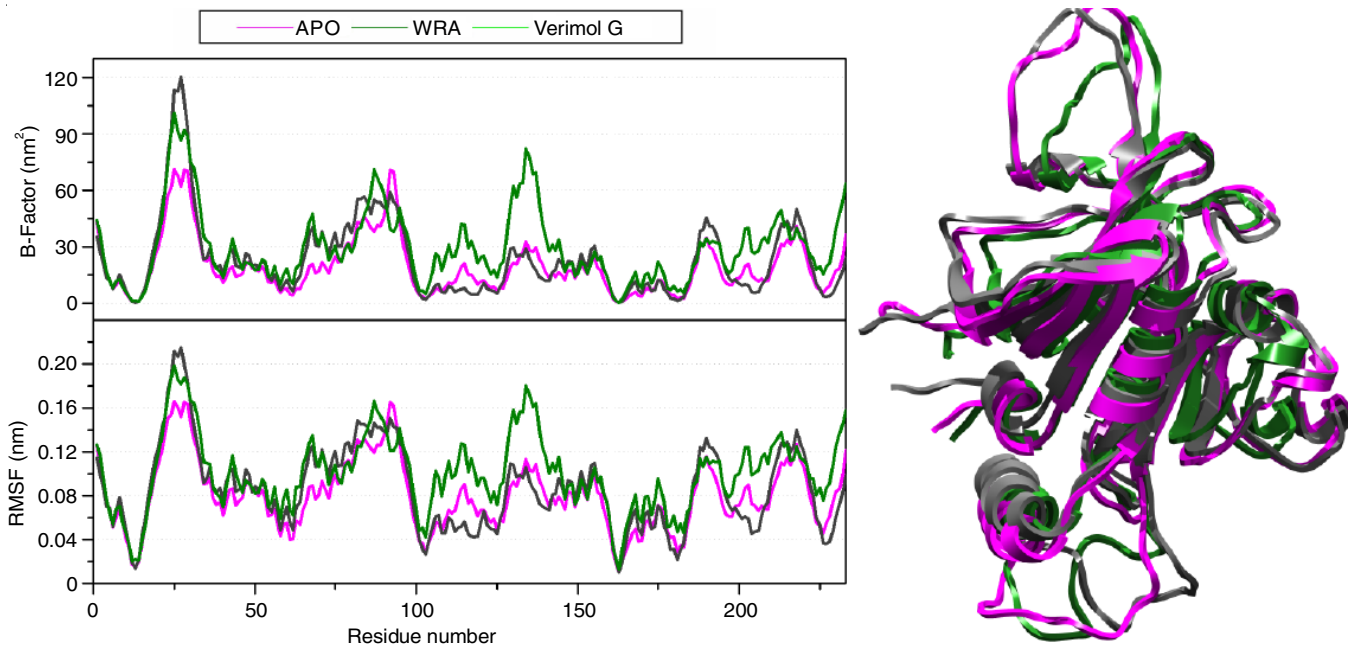

Fig. 4. The-root-mean-square-fluctuations (RMSF) and B-factor (left) and complex superposition (right) between APO (magenta), WRA (dark grey) and Verimol G (forest green) after MD simulation

(RMSF) and B-factor [29,30]. Based on Fig. 4, there is a correlation between RMSD and B-factor as some residues fluctuated significantly (R24-28, R82-87) in loop regions. The fluctuation indicated instability. It was anticipated because our attention was on the helix region, which served as an active site [31]. The loop regions exhibited higher RMSF values exceeding 0.14 nm and 90 ± 25 for B-factor, mostly due to the flexible nature of the β-strand structure. The minimum RMSF observed was 0.01 nm and 0.3 ± 0.5 in B-factor for each ligand and apoprotein with their complex. However, the RMSF and B-factor results showed that the complex ligand was stable enough and the conformation had low flexibility.

Key binding residues: Some key binding residues contributed to the stabilizing ligand binding, which was analyzed from free energy decomposition [32]. However, the energy decomposition ($\Delta G_{bind}^{residue}$) evaluation used the MM-GBSA model plotted over the last 10 ns trajectories. The $\Delta G_{bind}^{residue}$ analyses intend to evaluate the amino-acid interaction energy in the receptor active site. The interaction energy criterion is < -1 kcal/mol, where Fig. 5 shows all the key residues based on the criterion. The primary energy contributors of WRA were L46, I112, I14, C15 and F58; meanwhile, in verimol G, it was I112. The mentioned factors had a positive impact on the interaction and made a significant contribution to the overall free energy. Therefore, all the eligible residues could play a vital role in the binding pattern of the ligand receptor.

Inhibitor-wild-type *P. falciparum* interaction: In this analysis, we described the interaction based on two variables, atom contact and hydrogen bond, after 100 ns simulation [33]. The hydrogen bond appears from hydrogen and electronegative atom attraction [31]. The results (Fig. 6) show that verimol G has interacts less than WRA however, verimol G had intense contact only in the beginning 20 ns. Several 12 contacts in verimol G-PfDHFR and 11 in WRA-Pf were found. Based on

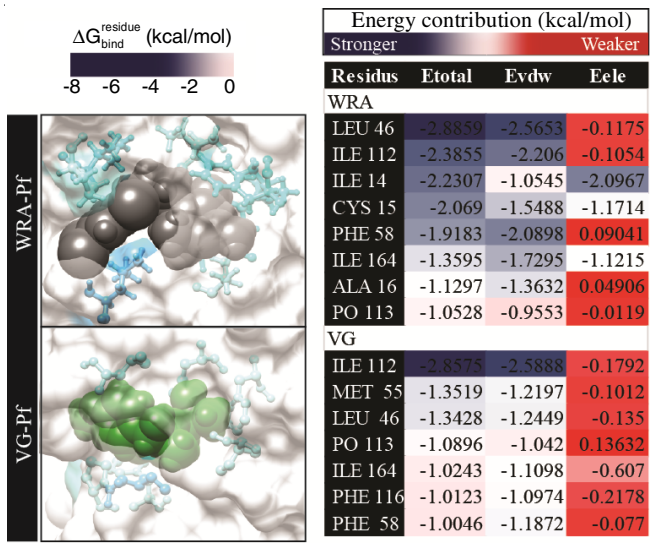

Residus	Etotal	Evdw	Eele
WRA			
LEU 46	-2.8859	-2.5653	-0.1175
ILE 112	-2.3855	-2.206	-0.1054
ILE 14	-2.2307	-1.0545	-2.0967
CYS 15	-2.069	-1.5488	-1.1714
PHE 58	-1.9183	-2.0898	0.09041
ILE 164	-1.3595	-1.7295	-1.1215
ALA 16	-1.1297	-1.3632	0.04906
PO 113	-1.0528	-0.9553	-0.0119
VG			
ILE 112	-2.8575	-2.5888	-0.1792
MET 55	-1.3519	-1.2197	-0.1012
LEU 46	-1.3428	-1.2449	-0.135
PO 113	-1.0896	-1.042	0.13632
ILE 164	-1.0243	-1.1098	-0.607
PHE 116	-1.0123	-1.0974	-0.2178
PHE 58	-1.0046	-1.1872	-0.077

Fig. 5. The energy decomposition and energy contribution (E_{vdW} + E_{ele}) analysis using MM-GBSA calculation from last-10-ns trajectory

residues on the binding side, the key binding residues having contact between candidates and the targeted complex were detected. During the 100 ns simulation, residues I14 and D54 in WRA and D54 in verimol G were the key residues. From the hydrogen occupation, the hydrogen bonding showed 62.34% in I14 and 40.93% in D54. On the other hand, verimol G-PfDHFR gave a percentage of 25% in residue D54, which has a low hydrogen bond cluster [34].

Conclusion

Verimol G was successfully isolated from the ethyl acetate extract of *Illicium* verum Hook. f. fruit. The isolated compound was tested computationally as antiplasmodial agent. The WRA, the native ligand of the receptor, was used as a positive control.

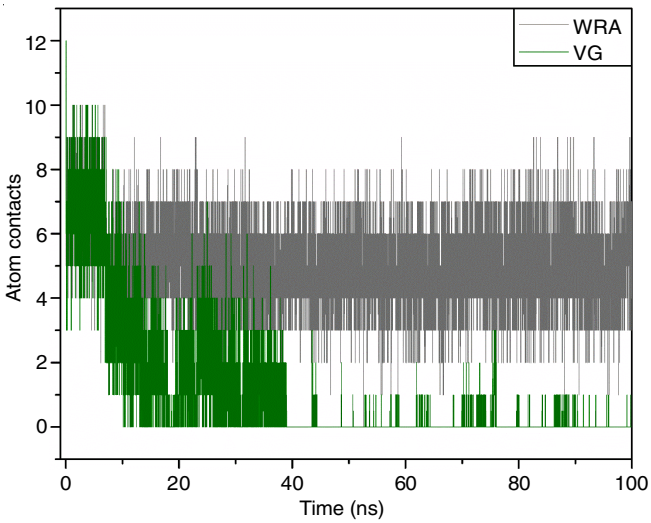

Fig. 6. Inhibitor-wild-type *P. falciparum* dihydrofolate reductase (PfDHFR) interaction: Atom contact through 100-ns simulation

Analysis of the findings revealed that WRA exhibited stronger inhibition compared to verimol G. Despite this, the potential of verimol G is still significant, especially considering the need for further exploration of the genus.

ACKNOWLEDGEMENTS

The authors are grateful to Department of Chemistry, Faculty of Science and Technology and UCoE Research Centre for Bio-Molecule Engineering and Bioinformatics, Universitas Airlangga (BIOME-UNAIR) to provide the research facilities. This research was funded through a scheme Penelitian Dasar Kompetitif Nasional (PDKN) from DRTPM KEMENDIKBUD-RISTEK TAHUN 2022. Contract Number : 919/UN3.15/PT/2022.

CONFLICT OF INTEREST

The authors declare that there is no conflict of interests regarding the publication of this article.

REFERENCES

1. G.-W. Wang, W.-T. Hu, B.-K. Huang and L.-P. Qin, *J. Ethnopharmacol.*, **136**, 10 (2011); https://doi.org/10.1016/j.jep.2011.04.051
2. Y.N. Liu, X.H. Su, C.H. Huo, X.P. Zhang, Q.W. Shi and Y.C. Gu, *Chem. Biodivers.*, **6**, 963 (2009); https://doi.org/10.1002/cbdv.200700433
3. Q. Zou, Y. Huang, W. Zhang, C. Lu and J. Yuan, *Molecules*, **28**, 7378 (2023); https://doi.org/10.3390/molecules28217378
4. Y. Huang, J. Zhao, L. Zhou, J. Wang, Y. Gong, X. Chen, Z. Guo, Q. Wang and W. Jiang, *Molecules*, **15**, 7558 (2010); https://doi.org/10.3390/molecules15117558
5. H. A. Bhatti, S. Khan, S. Faizi, G. Abbas, I. Ali, S. Jawaid, A.N.A. Ali, R. Jamy, F. Shahid, M.A. Versiani and A. Dar, *J. Anal. Pharm. Res.*, **6**, 177 (2017); https://doi.org/10.15406/japlr.2017.06.00177
6. H.N. Khan, S. Rasheed, M.I. Choudhary, N. Ahmed and A. Adem, *BMC Complement Altern. Med.* **22**, 79 (2022); https://doi.org/10.1186/s12906-022-03550-z
7. M. De, A.K. De, P. Sen and A.B. Banerjee, *Phytother. Res.*, **16**, 94 (2002); https://doi.org/10.1002/ptr.989
8. M.L. Willcox and G. Bodeker, *BMJ*, **329**, 1156 (2004); https://doi.org/10.1136%2Fbmj.329.7475.1156
9. E. O. Appiah, S. Appiah, E. Oti-Boadi, A. Oppong-Besse, D. B. Awuah, P. O. Asiedu and L. E. Oti-Boateng, *PLoS ONE*, **17**, 1 (2022); https://doi.org/10.1371/journal.pone.0271669
10. M.M. Taek, B. Prajogo and M. Agil, *Open Access J. Complement. Altern. Med.*, **1**, 76 (2019); https://doi.org/10.32474/OAJCAM.2019.01.000121
11. F.D. Prieto-Martínez, E. López-López, K.E. Juárez-Mercado and J.L. Medina-Franco, Computational Drug Design Methods—Current and Future Perspectives, In: Silico Drug Design: Repurposing Techniques and Methodologies, Academic Press: Cambridge-Massachusetts, USA, Chap. 2, pp. 19-44 (2019).
12. O. Osakwe and S. Rizvi, The Significance of Discovery Screening and Structure Optimization Studies, In: Social Aspects of Drug Discovery, Development and Commercialization, Elsevier, Chap. 5, pp. 109-128 (2016).
13. J.A. Maier, C. Martinez, K. Kasavajhala, L. Wickstrom, K.E. Hauser and C. Simmerling, *J. Chem. Theory Comput.*, **11**, 3696 (2015); https://doi.org/10.1021/acs.jctc.5b00255
14. A. Jakalian, D.B. Jack and C.I. Bayly, *J. Comput. Chem.*, **23**, 1623 (2002); https://doi.org/10.1002/jcc.10128
15. P.T. Lang, DOCK 6.1 Users Manual (2007).
16. A. Castro-Alvarez, A.M. Costa and J. Vilarrasa, *Molecules*, **22**, 136 (2017); https://doi.org/10.3390/molecules22010136
17. D.A. Case, T.E. Cheatham, T. Darden, H. Gohlke, R. Luo, K.M. Merz Jr., A. Onufriev, C. Simmerling, B. Wang and R.J. Woods, *J. Comput. Chem.*, **26**, 1668 (2005); https://doi.org/10.1002/jcc.20290
18. D.A. Case, Amber 2022 Reference Manual (2022).
19. K. Wichapong, A. Rohe, C. Platzer, I. Slynko, F. Erdmann, M. Schmidt and W. Sippl, *J. Chem. Inf. Model.*, **54**, 881 (2014); https://doi.org/10.1021/ci4007326
20. H. Hu, Z. Lu and W. Yang, *J. Chem. Theory Comput.*, **3**, 390 (2007); https://doi.org/10.1021/ct600240y
21. S. Endo and H. Wako, *Biophys Physicobiol.*, **16**, 205 (2019); https://doi.org/10.2142%2Fbiophysico.16.0_205
22. Q. Luo, C. Zhang, L. Miao, D. Zhang, Y. Bai, C. Hou, J. Liu, F. Yan, Y. Mu and G. Luo, *Amino Acids*, **44**, 1009 (2013); https://doi.org/10.1007/s00726-012-1435-3
23. Y. Cong, M. Li, G. Feng, Y. Li, X. Wang and L. Duan, *Scient. Rep.*, **7**, 17708 (2017); https://doi.org/10.1038/s41598-017-17868-z
24. E. Wang, H. Sun, J. Wang, Z. Wang, H. Liu, J.Z.H. Zhang and T. Hou, *Chem. Rev.*, **119**, 9478 (2019); https://doi.org/10.1021/acs.chemrev.9b00055
25. L.K. Sy and G.D. Brown, *J. Nat. Prod.*, **61**, 987 (1998); https://doi.org/10.1021/np9800553
26. S. Pérez and I. Tvaroška, *Adv. Carbohydr. Chem. Biochem.*, **71**, 9 (2014); https://doi.org/10.1016/B978-0-12-800128-8.00001-7
27. I.L. Lu and H. Wang, *J. Comput. Biol.*, **19**, 1215 (2012); https://doi.org/10.1089/cmb.2012.0188
28. H. Mirzaei, S. Zarbafian, E. Villar, S. Mottarella, D. Beglov, S. Vajda, I.C. Paschalidis, P. Vakili and D. Kozakov, *J. Chem. Theory Comput.*, **11**, 1063 (2015); https://doi.org/10.1021%2Fct500155t
29. Y.P. Pang, *Heliyon*, **2**, e00161 (2016); https://doi.org/10.1016/j.heliyon.2016.e00161
30. L. Martínez, *PLoS One*, **10**, e0119264 (2015); https://doi.org/10.1371/journal.pone.0119264
31. S. Robinson, A. Afzal and D.P. Leader, Bioinformatics: Concepts, Methods and Data, In: Handbook of Pharmacogenomics and Stratified Medicine, Academic Press, Cambridge-Massachusetts, USA, Chap. 3, pp. 259-287 (2014).
32. M.J.S. Phipps, T. Fox, C.S. Tautermann and C.K. Skylaris, *Chem. Soc. Rev.*, **44**, 3177 (2015); https://doi.org/10.1039/c4cs00375f
33. E. Nittinger, T. Inhester, S. Bietz, A. Meyder, K.T. Schomburg, G. Lange, R. Klein and M. Rarey, *J. Med. Chem.*, **60**, 4245 (2017); https://doi.org/10.1021/acs.jmedchem.7b00101
34. M. Simonèiè and T. Urbiè, *Chem. Phys.*, **507**, 34 (2018); https://doi.org/10.1016/j.chemphys.2018.03.036